BAYESIAN UPDATING OF PLANETARY ROVER WHEEL-SOIL CONTACT MODEL

A. Gallina[(1),(2)], R. Krenn[(1)], M. Scharringhausen[(3)], and B. Schäfer[(1)]

[(1)]*Deutsches Zentrum für Luft- und Raumfahrt, Institute of Robotics and Mechatronics, Germany, Email: alberto.gallina@dlr.de, rainer.krenn@dlr.de, bernd.schaefer@dlr.de*
[(2)]*AGH University of Science and Technology, Institute of Robotics and Mechatronics, Poland, Email: alberto.gallina@agh.edu.pl*
[(3)]*Deutsches Zentrum für Luft- und Raumfahrt, Institute of Space Systems, Germany, Email: marco.scharringhausen@dlr.de*

ABSTRACT

At present, most of existing contact models for sandy soils are based on Bekker′s theory. Bekker parameters are initially assessed through bevameter tests and subsequently used in the wheel-soil contact model. This strategy, although commonly accepted for practical reasons, disregards the substantial difference between bevameter plate-soil and wheel-soil contact scenario. In this paper an alternative procedure for wheel-soil contact model parameter estimation is presented. It makes use of bevameter tests along with single wheel experiments and integrates both experimental data within a Bayesian approach. The results of the Bayesian model updating are compared with those of a traditional updating procedure and bevameter measurements.

Key words: Planetary rover; Bayesian model updating; soil contact model.

1. INTRODUCTION

Computer simulations of rover mobility on sandy soil play an important role in extraterrestrial exploration programs. Past experience has shown that, when driving on sandy soil, the rover may get stuck for long time and, in the worst case, be unable to recover its mobility. One such famous example is closely connected with the NASA Mars rover Spirit, that got completely stuck after five years of very successful operations on Mars surface. Therefore, in the terramechanics community it is well accepted that a good knowledge of the wheel-soil contact interacting forces is a prerequisite for both reliable modelling and predictions of realistic behaviour for in-situ operations. At present, most of the existing contact models for sandy soils are based on Bekker′s theory. However, several concerns arise when applying Bekker′s approach to wheel-soil contact models. Bekker parameters, often assessed through bevameter tests, are proved to be highly sensitive to the test setup as for instance soil preparation, plate shape or velocity [1]. Thus, inherent variabilities in the testing process result in uncertainty about the values of the Bekker parameters. Furthermore, wheel-soil contact models employ these parameters regardless of the fact that the geometrical configuration of the wheel-soil contact is substantially different from that of a bevameter test. This gives also rise to doubts about the correctness of using the same soil parameter values in the soil-wheel contact model.

In this paper the soil parameters used in a Bekker-based wheel-soil contact model are assessed by means of bevameter and single wheel tests. Exploiting parameter values tailored to the wheel-soil contact scenario, more reliable simulations of the rover mobility are expected. Furthermore, Bayesian model updating introduces a different perspective with respect to classical deterministic model updating techniques. Conversely to these latter, that produce point estimates, Bayesian updating returns a set of solutions with different levels of plausibility. This allows the researcher to make more judicious decisions in condition of model and parameter uncertainty.

The paper is structured as follows. In Section 2 theoretical aspects of Bayesian model updating are presented. In Section 3 the algorithm used to compute the Bayesian procedure is introduced. Section 4 is devoted to explaining main modelling issues of the soil contact model employed in this work. A parameter estimation application case is described in Section 5. Final comments and perspectives on future work are given in Section 6.

2. BAYESIAN MODEL UPDATING

Model updating problem aims to estimate parameter values of a computer model using a limited set of experimental data. In a deterministic view of the problem, standard updating procedures search for the model configuration that produces the best agreement with the available experimental data. Unlikely, in a Bayesian framework a set of different models are identified as plausible and weighted according to the probability to explain experimental data.

Bayesian model updating (BMU) has its foundation in the famous Bayes′ rule stating that

$$P(A \mid B) = \frac{P(B \mid A)P(A)}{P(B)} \tag{1}$$

where $P(A)$ and $P(B)$ denote respectively the total probabilities of two events A and B, while $P(A \mid B)$ and $P(B \mid A)$ denote the two conditional probabilities that the event A is verified given that the event B is verified and vice-versa.

In order to read these probabilities in a model updating context it is initially assumed that a class of models $\mathfrak{M}(\boldsymbol{\theta})$ of the physical process is available, with $\boldsymbol{\theta}$ the model parameters vector. A specific model is defined once $\boldsymbol{\theta}$ is assigned. The model response $y(\boldsymbol{\theta})$ is also function of $\boldsymbol{\theta}$. In general the model response differs from the experimental response x for a gap $\epsilon(\boldsymbol{\theta})$ that is in turn function of $\boldsymbol{\theta}$. Thus, the following relation holds

$$x = y(\boldsymbol{\theta}) + \epsilon(\boldsymbol{\theta}) \tag{2}$$

The prediction error ϵ may be assumed to be a Gaussian random variable with mean equal to the model response $y(\boldsymbol{\theta})$ and assigned standard deviation σ. In the absence of any additional information, the choice of a Gaussian probability density function (PDF) for ϵ maximizes the model uncertainty, according to the principle of maximum entropy [2]. With this assumption the probability density of the response x for a given model with parameters $\boldsymbol{\theta}$ is

$$p(x \mid \boldsymbol{\theta}) = \frac{1}{\sqrt{2\pi}\sigma} \exp\left(-\frac{f(\boldsymbol{\theta})^2}{2\sigma^2}\right) \tag{3}$$

with

$$f(\boldsymbol{\theta}) = \epsilon(\boldsymbol{\theta}) = x - y(\boldsymbol{\theta}) \tag{4}$$

that measures the fitness of the model response to the experimental response. The PDF $p(x \mid \boldsymbol{\theta})$, also referred to as *likelihood function*, may more generally be written as $p(D \mid \boldsymbol{\theta})$, with D denoting now a set of experimental data. Since the model parameter values are initially unknown, they can be considered random variables with PDF $p(\boldsymbol{\theta})$. Thus, the distribution $p(\boldsymbol{\theta})$ represents the guess of the researcher about the model parameter values before observing or taking into account experimental data. For this reason it is also referred to as *prior distribution*. If prior information on $\boldsymbol{\theta}$ are scarce or non-existent, $p(\boldsymbol{\theta})$ has to be very wide and allow for any admissible configuration for $\boldsymbol{\theta}$. Once the experimental data D are available, the guess on the distribution of $\boldsymbol{\theta}$ can be enhanced. Thus, the prior distribution is corrected to the *posterior distribution* $p(\boldsymbol{\theta} \mid D)$ that is the conditional PDF of $\boldsymbol{\theta}$ for given experimental data D. Recalling the Bayes′ rule expression for the continuous random variable, prior and posterior distribution are related to each other by

$$p(\boldsymbol{\theta} \mid D) = \frac{p(D \mid \boldsymbol{\theta})p(\boldsymbol{\theta})}{p(D)} \tag{5}$$

with $p(D)$ representing the normalizing factor for the numeration on the right-hand side that can be calculated as

$$p(D) = \int_{\boldsymbol{\Theta}} p(D \mid \boldsymbol{\theta})p(\boldsymbol{\theta})\, d\boldsymbol{\theta} \tag{6}$$

with $\boldsymbol{\Theta}$ the domain of $\boldsymbol{\theta}$. If both sides of Equation (5) are multiplied by $dDd\boldsymbol{\theta}$, then the PDFs can be written as probabilities and the formula becomes equivalent to Equation (1). Thus, the following interpretation is given: when considering experimental data, the probability of the event that the model parameter values takes the values $\boldsymbol{\theta}$ is proportional to the weighted likelihood of observing data D with a model with parameters $\boldsymbol{\theta}$ and weights given by the prior PDF $p(\boldsymbol{\theta})$. Importantly, the posterior distribution should not be read in a frequentist sense, i.e. as the frequency of occurrence of $\boldsymbol{\theta}$ for a given dataset D. If $p(\boldsymbol{\theta}' \mid D) > p(\boldsymbol{\theta}'' \mid D)$, it does not mean that $\boldsymbol{\theta}'$ is occurring more frequently than $\boldsymbol{\theta}''$ but that the event $\boldsymbol{\theta} = \boldsymbol{\theta}'$ explains better experimental evidence and parameter prior information than the event $\boldsymbol{\theta} = \boldsymbol{\theta}''$. In other words, $\mathfrak{M}(\boldsymbol{\theta}')$ is a more plausible model than $\mathfrak{M}(\boldsymbol{\theta}'')$. For a comprehensive description of Bayesian approach in model updating see [2].

3. TRANSITIONAL MARKOV CHAIN MONTE CARLO

The posterior distribution in Equation (5) may be calculated employing sampling strategies that ensure the probabilities to asymptotically converge toward correct estimates. However, there are several numerical challenges related to the usage of sampling-based methods. Firstly, since $p(\boldsymbol{\theta} \mid D)$ is usually very peaked, then a sampling approach results effective as long as a large number of samples stay in the neighbourhood of the important (but unknown) region of the parameter space. Secondly, accurate calculation of the normalization factor $p(D)$ by crude Monte Carlo method is, in general, numerically too expensive and requires an infeasible number of samples. An efficient approach for Bayesian model updating has been recently proposed in [3]. The method is an advanced Markov Chain Monte Carlo (MCMC) algorithm called Transitional Markov Chain Monte Carlo (TMCMC). Besides the advantage of a traditional MCMC [4] that avoids the calculation of the normalization factor, in TMCMC a sequence of Bayes' problems is solved where the posterior distribution of the former step is used as prior distribution in the next step and the amount of exploited experimental data is gradually increased. This step by step approach, resembling the simulated annealing method, favours the movement of the posterior distribution toward highly important regions of the parameter space. A detailed description of TMCMC along with its statistical properties is provided in [3].

4. SOIL CONTACT MODEL

The wheel-soil interaction dynamics implementation is based on the soil contact model (SCM) [5], which is dedicated for multi-body dynamics simulation applications. It computes the contact forces and torques between an arbitrarily shaped contact body and a soft terrain surface

as function of the body's motion state. The parameters are the CAD-like surface descriptions of body and terrain and the relevant soil properties. The aim of the implementation is basically the transformation of Bekker's semi-empirical terramechanics theory, which is derived from 1D/1DOF penetration tests with cylindrical probes, to general applications using arbitrarily shaped bodies in 3D with six degrees of freedom. The tool provides two main functionalities, which are performed at each time integration step of the simulation: the contact dynamics computation according to Bekker and the plastic soil deformation as function of surface penetration kinematics. Main features of these two functionalities are described in the following subsections.

4.1. Contact dynamics computation

The first computational step is contact detection. Using a digital elevation model (DEM) $\mathbf{z}_{DEM} = f(\mathbf{x}_{DEM}, \mathbf{y}_{DEM})$ for soil surface description and a cloud of points for representing the contact body surface, one can easily compute the sinkage profile from the contact footprint depth $\mathbf{z}_i$ at each contact node i of the soil DEM $(\mathbf{x}_i, \mathbf{y}_i)$. $\mathbf{z}_i$ are calculated by z-buffer and spatial binning techniques, which are well known in computer graphics. The corresponding contact velocities $\mathbf{v}_i$, which consist of components $\mathbf{v}_{\sigma,i}$ normal to the footprint surface and components $\mathbf{v}_{\tau,i}$ tangential to it, are computed by basic kinematics relationships.

From the knowledge about the footprint shape the effective contact width is calculated as $b_{eff} = 2A_{xy}/L_{xy}$ where A_{xy} is the projected footprint area and L_{xy} the projected contour length. A further aspect to be considered is the centrality of each contact node within the footprint. For this purpose a sinkage-independent pressure distribution function $\gamma(x_i, y_i)$ is defined. It acts as weighting factor that amplifies the nominal sinkage-dependent pressure in central footprint regions and let it drop down to zero at the border.

In the third step all computations are contact node specific only. Applying Bekker's pressure-sinkage relationship the contact pressure p_i, equal to the normal stress σ_i acting on the wheel, is

$$p_i = \gamma_i \left(\frac{k_c}{b_{eff}} + k_\phi \right) z_i^n \tag{7}$$

with the soil parameters cohesive modulus k_c, frictional modulus k_ϕ and exponent of sinkage n. Since the applicable shear stress is limited according to Mohr/Coulomb by $\tau_{max,i} = c + p_i \tan\Phi$ with soil cohesion c and angle of internal soil friction Φ, the actually applied shear stress,

$$\tau_i = \tau_{max,i} \left(1 - \exp^{-|\mathbf{v}_{\tau,i}|/v_0} \right), \tag{8}$$

is computed by an exponential function of the relative shear velocity $|\mathbf{v}_{\tau,i}|/v_0$ with v_0 a reference soil velocity parameter. The discrete contact force $\Delta\mathbf{F}_i$ can be expressed using the local normal vector $\mathbf{n}_i$, the corresponding tangent vector $\mathbf{t}_i = \mathbf{v}_{\tau,i}/|\mathbf{v}_{\tau,i}|$ and the discrete footprint size ΔA_i associated with a contact node by

$$\Delta\mathbf{F}_i = (\sigma_i \mathbf{n}_i + \tau_i \mathbf{t}_i)\, \Delta A_i. \tag{9}$$

The total contact force $\mathbf{F}$ and torque $\mathbf{T}$ are finally obtained by integrals of $\Delta\mathbf{F}_i$ over all N contact nodes with

$$\mathbf{F} = \sum_{i=1}^{N} \Delta\mathbf{F}_i \quad \text{and} \quad \mathbf{T} = \sum_{i=1}^{N} \left((x_i, y_i, z_i)^T \times \Delta\mathbf{F}_i \right). \tag{10}$$

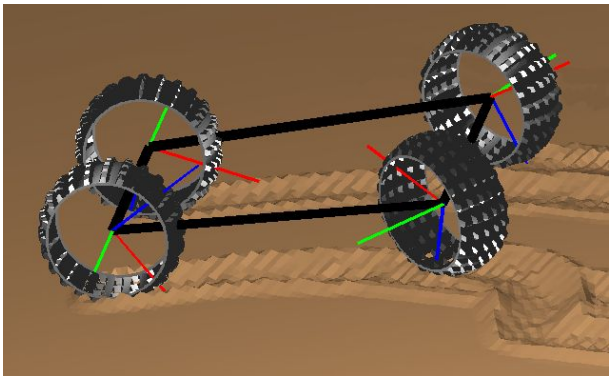

Figure 1. Visualization of rover locomotion simulation result using SCM

4.2. Plastic Soil Deformation

In order to represent typical terramechanics phenomena like sinkage, bulldozing, digging and multi-pass effects of wheels rolling in line an algorithm for plastic soil deformation is implemented in SCM (see example in Figure 1). It updates the DEM shape in each simulation step for consecutive application in the contact dynamics computation (see 4.1). Unlike discrete element based algorithms, SCM does not explicitly compute the soil particle dynamics. This latter is approximated by contact velocity dependent soil flow fields that determine the displacement of soil volume from the current contact footprint (decreasing DEM elevation) and the deposition of soil around the footprint border (rising DEM elevation). An algorithm for thermal erosion keeps the DEM surface in a natural shape considering the maximum angle of repose.

5. APPLICATION CASE

The application case consists of the parameter identification problem of a rigid-body model using SCM to simulate the motion of a wheel on sandy soil. Experimental results from a single wheel test (SWT) and Bevameter tests are provided by the DLR Institute of Space Systems in Bremen.

5.1. Experimental tests

The single wheel test facility allows tests of planetary or terrestrial rover wheels on different types of soil. The wheel is driven by a sled through the soil bin (see Figure 2). The soil bin itself is 300 x 60 x 50 cm, but it is divided into two parts filled with two different types of soil. Thus, a total length of 1.5 m is available for test runs. All relevant locomotion parameters are recorded with 10 Hz frequency during a test run:

- Drawbar pull (0 - 100 N)
- Torque (0 - 30 N)
- Sinkage (maximal sinkage depending on wheel size)
- Wheel load (0 - 200 N)
- Wheel and sled velocity (0 - 100 mm/s)
- Slippage (−100 - 100 %)

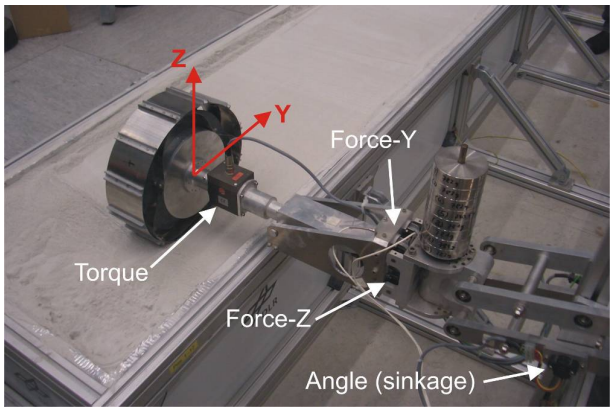

Figure 2. Single wheel test bed

The slippage is commanded by differential speeds of the sled and the wheel. Tests with free wheels are possible as well.

The wheel tested in the facility is a flexible wheel designed for the ESA ExoMars project. Its geometric properties are a nominal radius of 125 mm, width of 112 mm and 12 straight grousers with 9 mm depth. The soil is a dry quartz sand named WF34. The major chemical constituent of this sand is SiO2 (99.7%) comprising almost exclusively grains of sizes between 180 and 355 μm (80%). Minor constituents are grains of sizes between 125 and 180 μm. The bulk density has been measured to be approximately 1400 kg/m^3. Bevameter tests of WF34 measured the soil cohesion $c \approx 0$ Pa, friction angle $\Phi \approx 30°$, soil deformation exponent $n \approx 1.1$ and soil deformation modulus $k^* \approx 10^7$ N/m^{n+2}. k^* is related to the Bekker coefficients k_c and k_ϕ appearing in Equation (7) through

$$k^* = \left(\frac{k_c}{b_{eff}} + k_\phi \right) \tag{11}$$

5.2. Computer model

A rigid-body model using SCM has been created with the commercial software SIMPACK to simulate the SWT (Figure 3). The rigid-body model resembles the experimental set-up except for the flexible wheel that is assumed to be rigid in the simulation. The elastic deformation of the real wheel is accounted for in the simulation by a wheel with increased radius. However, since the wheel deformation is not measured during the experiment, the equivalent radius of the rigid wheel R is one of the parameters to identify. Other parameters are the soil properties k_c, k_ϕ, n, Φ used in SCM. Remaining SCM soil parameters are fixed because they are expected not to sensibly influence the results. Prior knowledge on the soil parameter values is provided by the Bevameter tests. Here, it seems important to stress that for k_c and k_ϕ no nominal value exists as an infinite number of solutions are possible for given k^*. The epistemic character of the k_c and k_ϕ uncertainty has been considered by choosing uniform prior PDFs. The same goes for R. For n and Φ normal distributions have been chosen as prior PDFs. Proposed prior distributions and possible range of variation of all tuners are listed in Table 1. In the table header Par1 and Par2 stand for the mean (minimum value) and standard deviation (maximum value) of the normal (uniform) distribution, respectively, while LB and UB denote the lower and upper bound of the parameter space.

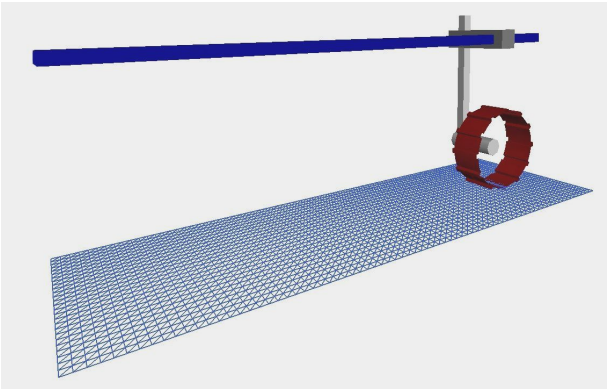

Figure 3. Rigid-body model of the single wheel test

Param	Dim	Dist	Par1	Par2	LB	UB
k_c	$[N/m^{n+1}]$	uniform	-10^9	10^9	-10^9	10^9
k_ϕ	$[N/m^{n+2}]$	uniform	1	10^{10}	1	10^{10}
n	$[-]$	normal	1.1	0.2	0.8	2
Φ	$[°]$	normal	30	5.7	11.5	37.3
R	$[m]$	uniform	0.125	0.155	0.125	0.155

Table 1. Prior distributions and parameter space definition.

5.3. Model updating procedures

The SWT data used to update the model parameters are the drawbar pull force F, the torque at the wheel hub T and the sinkage of the wheel z at constant slip value $s = 0.2$. The analysis of experimental data shows that after an initial transient, F, T and z get fluctuating around a mean value with oscillations caused by the wheel grousers. Since SCM is not able to exactly describe the transient behaviour, the prediction error (see Equation (4)) is defined as the difference between the experimental and numerical signal averages after an assigned transient. For the experiments the transient is set to 40 s while for the numerical data is 20 s for F and T and 1 s for z. Simulated time is 50 s while real experimental time is about 180 s. Referring to a generic dataset, Figure 4 illustrates the filtered experimental and numerical data and the resultant data averages (thick solid lines) used in BMU. The shaded areas in pale blue and red highlight the time interval over which the signal is averaged for experimental and numerical data, respectively. The diagrams show only first 100 s of experimental signal.

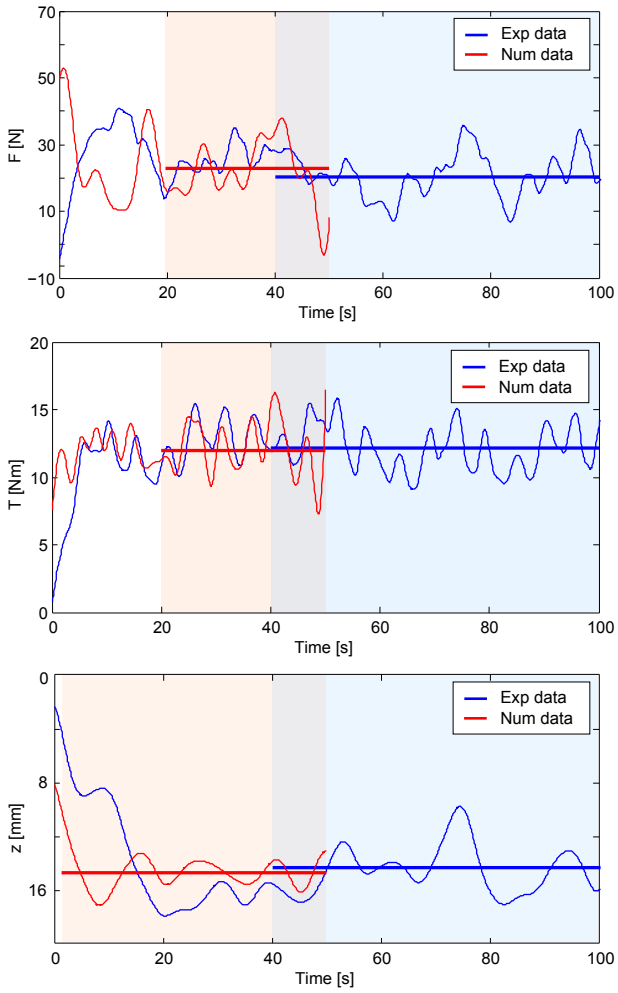

Figure 4. Filtered signals of experimental and numerical data (for a correct interpretation of this figure see the electronic version of the paper).

The likelihood function of Equation (5) is here defined as

$$p(D \mid \boldsymbol{\theta}) = \prod_{i=1}^{3} p(D_i \mid \boldsymbol{\theta}) \tag{12}$$

with

$$p(D_1 \mid \boldsymbol{\theta}) = \frac{1}{\sqrt{2\pi}} \exp\left(-\frac{(\bar{F}^{exp} - \bar{F}^{num})^2}{2\sigma_F^2}\right) \tag{13}$$

$$p(D_2 \mid \boldsymbol{\theta}) = \frac{1}{\sqrt{2\pi}} \exp\left(-\frac{(\bar{T}^{exp} - \bar{T}^{num})^2}{2\sigma_T^2}\right) \tag{14}$$

$$p(D_3 \mid \boldsymbol{\theta}) = \frac{1}{\sqrt{2\pi}} \exp\left(-\frac{(\bar{z}^{exp} - \bar{z}^{num})^2}{2\sigma_z^2}\right) \tag{15}$$

and $\bar{\bullet}^{exp}$, $\bar{\bullet}^{num}$ and $\sigma_\bullet$ being respectively the experimental, numerical mean and prediction error standard deviation of the generic physical quantity $\bullet$. The prediction error standard deviations are assumed to be constant values and play here the role of normalization factors to account for different order of magnitudes for the physical quantities. But, their value affects also the prediction error distribution, as will be discussed later.

Bayesian model updating has been compared with a deterministic parameter identification procedure that solves the inverse problem by a genetic algorithm (GA) optimization [6]. In this case the optimization searches for the global minimum of a defined objective function $g(\boldsymbol{\theta})$ over the assigned parameter space. The objective function is strictly related to the likelihood function of the Bayesian approach being

$$g(\boldsymbol{\theta}) = \log p(D \mid \boldsymbol{\theta}) \tag{16}$$

where $p(D \mid \boldsymbol{\theta})$ is defined in Equation (12).

5.4. Analysis of results

Both BMU and GA procedures are sequential algorithms that converge to a solution after an established number of steps. The converging error diagram for GA optimization is shown in the top diagram of Figure 5, while the samples of the initial, intermediate and final step of TMCMC are shown in the bottom scatter plot of Figure 5 in terms of n and Φ model parameters. In this latter plot it is visible that the initial prior sampling region is progressively shrunk and moved toward more probable parameter configurations by the random walk of TMCMC. At the end of the procedure almost all samples are clustered within a small region with $n \approx 1.2$ and $\Phi \approx 11.5°$.

As opposed to GA optimization, that yields point estimates, BMU supplies a collection model configurations with their corresponding level of plausibility. In Figure 6 the two-variate posterior densities are plotted as contour plots for k_c-k_ϕ, n-Φ and n-R pairs via the constant window kernel density estimators method [7]. The plots show also the TMCMC sample with maximum likelihood (or minimum prediction error), the GA optimum and, whenever

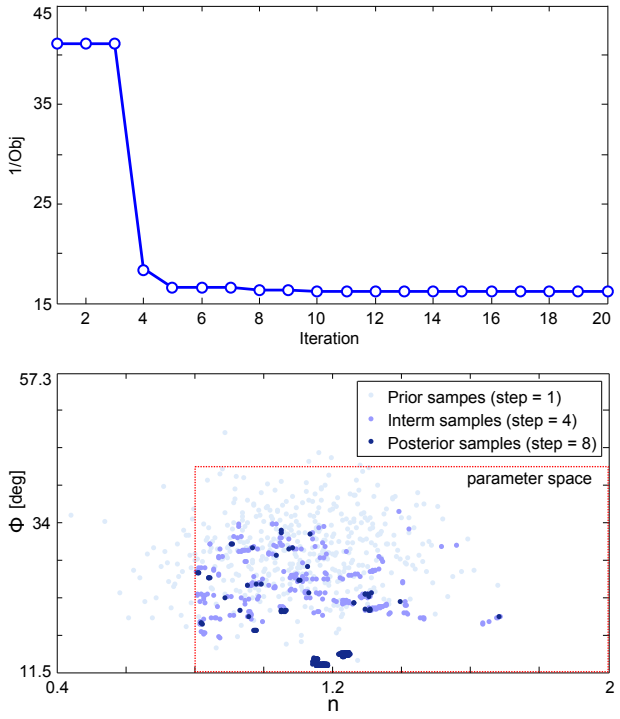

Figure 5. GA (top) and TMCMC (bottom) convergence.

possible, bevameter measurements. With a slight abuse of interpretation, the sample with maximum $p(D \mid \boldsymbol{\theta})$ is here denoted by MLE (maximum likelihood estimator). MLE is always located very close to the posterior PDF mode. This is a positive fact meaning that the value of $\boldsymbol{\theta}$ which minimizes the error is not a spurious peak but within the region of highly plausible models. In agreement with BMU, the k_ϕ, n and Φ identified by GA lie inside the region with very high posterior PDF values. On the other hand, k_c and R estimates are substantially away from the important posterior PDF regions. This is most likely due to the minor influence that these parameters have on the measured model responses.

It may convey also much insight about the SCM behaviour the comparison between numerical results and experimental bevameter measurements. In the plot on the top of Figure 6 the dashed line marks the k_c-k_ϕ combinations for which $k^* = 10^7$ N/m^{n+2} and setting b_{eff} to the average value from the simulations. As visible, the dashed line passes through high values of the posterior PDF. Moreover, the k_c-k_ϕ negative correlation is also caught by the posterior distribution. Both facts point out a sufficient experimental/numerical correlation. As far as n and Φ is concerned, the plot in Figure 6 shows that, while for n again a good experimental/numerical agreement exists, for Φ all numerical solutions concentrate in a region with sensibly smaller values than the bevameter measurement. Although the causes of such a strong disagreement are not clear yet, at the moment this result advices the researcher against an indiscriminate use in SCM of soil parameter estimates coming from bevameter tests.

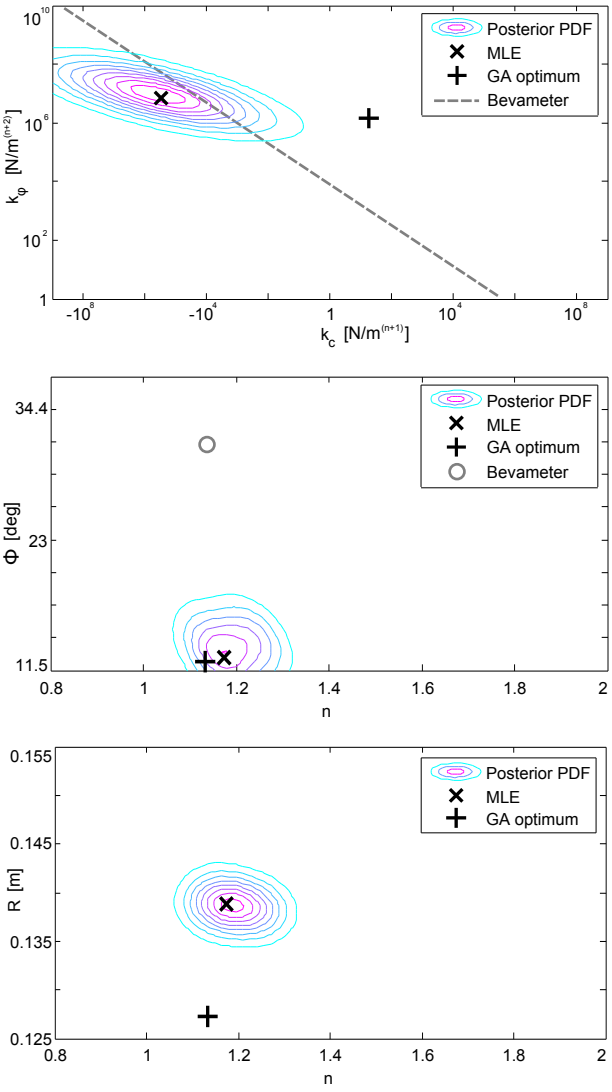

Figure 6. BMU and GA estimated parameters along with bevameter measurements.

The comparison of the F, T and z filtered time-histories for MLE and GA solution with the filtered experimental signal from SWT is presented in Figure 7. The plots show a very good experimental/numerical agreement in terms of signal averages (see the small diagrams on the right) and amplitude of fluctuation. Also the period behaviour due to the grousers is caught in the numerical solution.

BMU may provide also information about the prediction error variability. Figure 8 presents the calculated absolute prediction error PDFs of F, T and z built via kernel estimator with normal smoothers and optimal width for normal densities on a positive support. Vertical blue, red and green dashed lines are also drawn to mark the absolute prediction error mean, the error of the MLE solution and the error of the GA solution, respectively. These plots point out two important results. The first is qualitative and says that the prediction error yielded by MLE (or GA) is sensibly different from that expected when considering model uncertainty. The second is quantita-

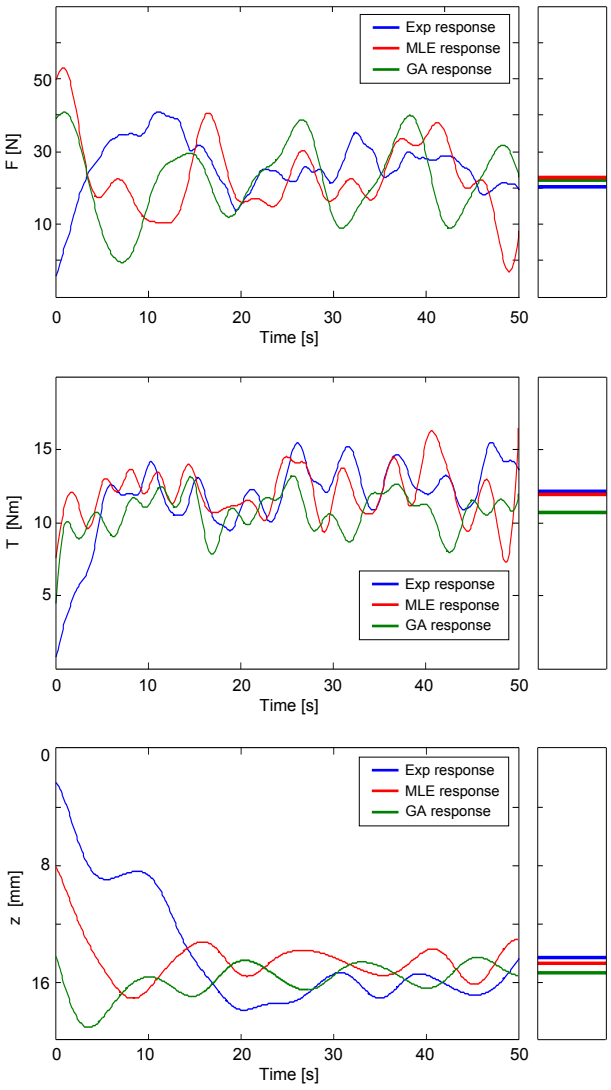

Figure 7. Experimental-numerical correlation for MLE and GA solution (for a correct interpretation of this figure see the electronic version of the paper).

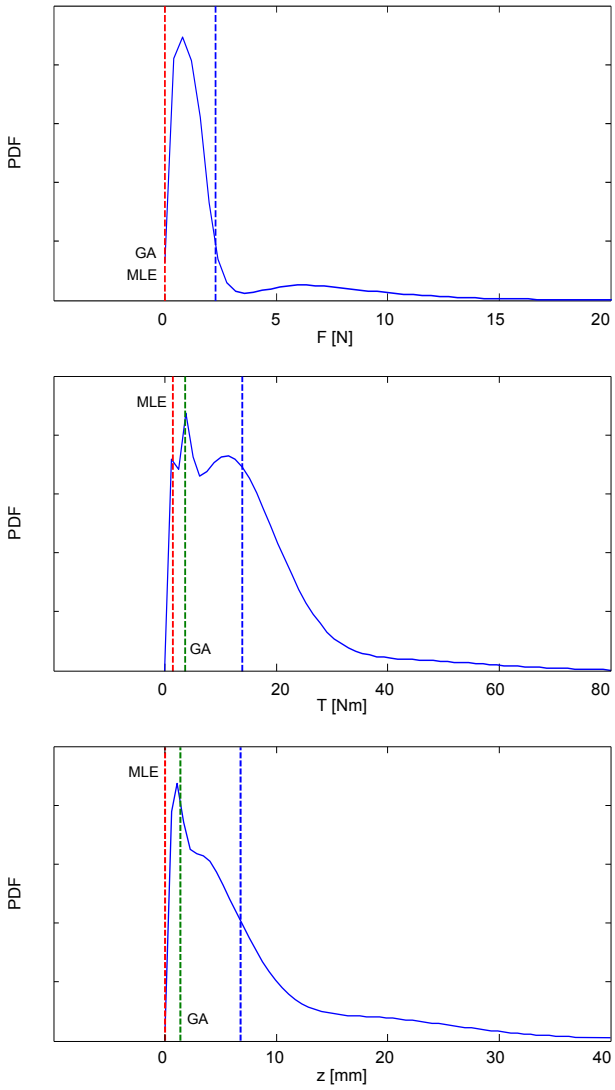

Figure 8. Prediction error distributions MLE and GA point estimates (for a correct interpretation of this figure see the electronic version of the paper).

tive and says that, globally, the prediction error is significantly larger than the MLE (or GA) estimate. In this regards, it seems important to note that the width of the error PDFs is dependent on the error standard deviation σ chosen for Equation (13). Current values are $\sigma_F = 10$ N, $\sigma_T = 20$ Nm and $\sigma_z = 0.01$ m that are chosen considerably large as to reduce the number of TMCMC samples. Indeed, due to statistical properties of TMCMC, the number of required simulations, needed to achieve reliable statistic, increases accordingly with the number of TMCMC samples. Conveniently, prediction error standard deviations may also be included into the set of parameters to estimate. Nevertheless, also this set-up would entail an augmented number of simulations that could not be afforded in the present work.

6. CONCLUSIONS

Conversely to traditional deterministic model updating that yields parameter point estimates, Bayesian framework gives a more robust approach by identifying a set of high plausible models. If integrating this information into a decision theory framework that minimizes the expected loss, then the full power of the Bayesian approach can be exploited. Furthermore, since handling flow of information is made in a very natural way, it is expected that Bayesian approach could be employed efficiently for on-time parameter estimation. Yet, by calculating the evidence distribution, Bayesian approach may be useful for model comparison and selection [8]. On the downside, Bayesian analyses generally call for high computer performances. In this work, parallel computing technique and efficient MCMC methods have been adopted. Nevertheless, the procedure, run on a machine equipped with

a 8-core and 2.8 GHz CPU, took several hours and required a number of simulations significantly larger than a deterministic approach. In this regard metamodelling techniques can be resorted to sensibly speed up the analysis, as proposed for instance by [9] in the context of a structural dynamic problem.

Focusing on the values of Bekker parameters identified by both of the updating procedures, it turns out that, in general, the updated estimates are in agreement with the bevameter measurements. An exception is the friction angle whose estimates are sensibly smaller. Additional simulations evidenced that for $\Phi \approx 30^\circ$ the numerical values for F and T are constantly pretty higher than the experimental values. This outcome suggests to pay particular attention when using bevameter data in SCM.

REFERENCES

[1] M. Apfelbeck, S. Kuss, B. Rebele, and B. Schaefer. A systematic approach to reliably characterize soils based on bevameter testing. *Journal of Terramechanics*, 48(5):360–371, 2011.

[2] J.L. Beck and L.S. Katafygiotis. Updating models and their uncertainties. part i: Bayesian statistical framework. *Journal of Engineering Mechanics*, 124:455–461, 1998.

[3] J. Ching and Y. Chen. Transitional markov chain monte carlo method for bayesian model updating, model class selection, and model averaging. *Journal of Engineering Mechanics*, 133(7):816–832, 2007.

[4] C. Andrieu, N. de Freitas, A. Doucet, and M.I. Jordan. An introduction to mcmc for machine learning. *Machine Learning*, 50(1-2):5–43, 2003.

[5] R. Krenn and A. Gibbesch. Soft soil contact modeling technique for multi-body system simulation. In Giorgio Zavarise and Peter Wriggers, editors, *Trends in Computational Contact Mechanics*, volume 58 of *Lecture Notes in Applied and Computational Mechanics*, pages 135–155. Springer Berlin / Heidelberg, 2011.

[6] Z. Michalewicz. *Genetic Algorithms + Data Structures = Evolution Programs*. Springer-Verlag, 1999.

[7] C.M. Bishop. *Pattern recognition and machine learning*. Springer, 1st ed. 2006. corr. 2nd printing edition, October 2006.

[8] M. Muto and J.L. Beck. Bayesian updating and model class selection for hysteretic structural model using stochastic simulation. *Journal of Vibration and Control*, 14:7–34, 2008.

[9] B. Goller, M. Broggi, A. Clavi, and G. Schueller. Efficient model updating of the goce satellite based on experimental modal data. In *Proceedings of COMPDYN2011*, 2011.